Atmos. Meas. Tech. Discuss., 6, 3059–3088, 2013
www.atmos-meas-tech-discuss.net/6/3059/2013/
doi:10.5194/amtd-6-3059-2013

Atmospheric Measurement Techniques
Discussions
Open Access

Retrieval of height-temporal distributions of particle parameters from multiwavelength lidar measurements using linear estimation technique and comparison results with AERONET

I. Veselovskii[1], D. N. Whiteman[2], M. Korenskiy[1], A. Kolgotin[1], O. Dubovik[3], and D. Perez-Ramirez[2,4]

[1]Physics Instrumentation Center of General Physics Institute, Troitsk, Moscow Region, 142190, Russia
[2]Mesoscale Atmospheric Processes Laboratory, NASA GSFC, Greenbelt, MD 20771, USA
[3]Laboratoire d'Optique Atmospherique, CNRS Universite de Lille 1, Bat P5 Cite scientifique, 59655 Villeneuve d'Ascq Cedex, France
[4]Applied Physics Department, University of Granada, 18071 Granada, Spain

Received: 10 March 2013 – Accepted: 13 March 2013 – Published: 28 March 2013

Correspondence to: I. Veselovskii (igorv@pic.troitsk.ru) and
D. N. Whiteman (david.n.whiteman@nasa.gov)

Published by Copernicus Publications on behalf of the European Geosciences Union.

Abstract

The results of application of the linear estimation technique to multiwavelength Raman lidar measurements performed during the summer of 2011 in Greenbelt, MD, USA are presented. We demonstrate that multiwavelength lidars are capable not only of providing vertical profiles of particle properties but also of revealing the spatio-temporal evolution of aerosol features. The night-time $3\beta + 1\alpha$ lidar measurements on 21 and 22 July were inverted to spatio-temporal distributions of particle microphysical parameters, such as volume, number density, effective radius and the complex refractive index. The particle volume and number density show strong variation during the night while the effective radius remains approximately constant. The real part of the refractive index demonstrates a slight decreasing tendency in a region of enhanced extinction coefficient. The linear estimation retrievals are stable and provide 2 min resolution time series of particle parameters at different heights. AERONET observations are compared with multiwavelength lidar retrievals showing good agreement.

1 Introduction

Multiwavelength (MW) Raman and HSRL aerosol lidars are recognized as powerful tools for aerosol characterization. The height resolved particle backscattering, extinction and depolarization at multiple wavelengths provided by such lidars can be used for aerosol classification (Omar et al., 2009; Burton et al., 2012) and are important parameters in climate modeling (Ganguly et al., 2008; Miller et al., 2011). Another attractive feature of these lidars is the ability to invert the measurements to provide vertical profiles of particle physical properties. During the last decade numerous theoretical and experimental studies have been performed attempting to realize such inversions and the results obtained look rather promising (Ansmann and Müller, 2005; Böckmann et al., 2005; Veselovskii et al., 2002, 2004, 2009, 2010, 2012; Müller et al., 1999, 2011; Noh et al., 2011). Though the amount of independent observations provided by MW

AMTD
6, 3059–3088, 2013

lidar technique is very limited (normally only three backscattering and two extinction coefficients are available) the use of reasonable constraints in the inversions allows the estimation of the particle characteristics. The potential of the method has also been extended due to recent progress in the treatment of desert particles and dust-smoke mixtures (Dubovik et al., 2006; Veselovskii et al., 2010; Tesche et al., 2009; Nishizawa et al., 2011).

To contribute to the study of the Earth radiation balance, the MW lidar measurements should be performed on a global scale thus space-borne systems are desirable. The operation of the CALIOP instrument since 2006 (Winker et al., 2009) has confirmed the potential of space lidar observations for aerosol classification and transport studies (Omar et al., 2009). The CALIOP instrument exploits just two (532 and 1064 nm) backscattering channels in combination with depolarization measurements at 532 nm, thus the next logical step would be to increase the number of the wavelengths and incorporate HSRL channels to provide a dataset that could support inversions to retrieve particle microphysics. The recent results obtained with the airborne NASA/LaRC HSRL system (Hair et al., 2008; Burton et al., 2012) support the importance of MW lidars measurements from space and today the ACE mission involving a $3\beta+2\alpha$ HSRL system is under consideration (http://dsm.gsfc.nasa.gov/ace).

However before transferring MW lidar technology to space, numerous issues in the analysis of the measurements should be resolved. In particular, the variability of aerosol parameters over the globe should be taken into account: the particles may be of irregular shape, the complex refractive index may be size and spectrally dependent and the aerosols may be represented by external or internal mixtures. Thus, to determine realistic uncertainties of the retrieved particle parameters numerous measurements at different locations are needed with the results being compared with independent collocated instruments. And finally, given that measurements from the space are generally characterized by higher uncertainties than ground-based measurements, the retrieval algorithms used for space-based measurements should be tolerant to measurement noise and fast enough to manage large volumes of data.

AMTD
6, 3059–3088, 2013

Retrieval of height-temporal distributions of particle parameters

I. Veselovskii et al.

Most commonly for inversion of MW measurements the regularization algorithm is used (Müller et al., 1999; Veselovskii et al., 2002, 2004), allowing the retrieval of particle size, concentration, complex refractive index (CRI), and to some extent the main features of the particle size distribution (PSD). However, the regularization methods are quite time consuming, so it is attractive to test other inversion techniques as possible candidates for operational algorithms for space-based data. One of the possible approaches to the inversion is based on the expansion of PSD in terms of the measurement kernels (Twomey, 1977; Thomason and Osborn, 1992; Donovan and Carswell, 1997; Veselovskii et al., 2012). The particle bulk properties in the frame of this approach are represented by a linear combination of the input optical data, so here and below we will refer to it as "linear estimation". The regularization and the linear estimation (LE) techniques are characterized by similar uncertainties (Veselovskii et al., 2012), but the LE technique is faster because there is no need to solve the system of linear equations for different values of predefined regularization parameters (Veselovskii et al., 2002, 2012). Application of this approach to measurements performed in Turkey (Veselovskii et al., 2012) has demonstrated stability of retrieval and the possibility of obtaining the time series of particle parameters.

In this paper we extend our previous study (Veselovskii et al., 2012) by applying the LE approach to the extended measurements performed with MW Raman lidar at NASA GSFC in Greenbelt, MD during the summer of 2011 to evaluate spatio-temporal distributions of particle parameters. To validate the technique the lidar retrievals are compared with the results provided by AERONET (Holben et al., 1998).

2 Approach to retrieval

The aerosol extinction (α) and backscattering coefficients (β) are related to the particle size distribution (PSD) $\frac{\mathrm{d}V(r)}{\mathrm{d}r}$ via integral equations as follows:

AMTD
6, 3059–3088, 2013

$$g_p = \int_{r_{\min}}^{r_{\max}} K_p(m,r)\frac{\partial V(r)}{\partial r}\mathrm{d}r \quad p = (i,\lambda_k) = 1,\ldots,N_0. \tag{1}$$

The index p represents the type of optical data ($i = \alpha$, β) and wavelengths λ_k; $K_p(m,r)$ are the volume kernels (VK) depending on the complex refractive index $m = m_\mathrm{R} + i \cdot m_\mathrm{I}$ and particle radius $r \in [r_{\min}, r_{\max}]$.

A detailed description of the linear estimation approach is given in Veselovskii et al. (2012). Equation (1) can be rewritten in the matrix–vector form. The vector of input optical data $\boldsymbol{g}$ (aerosol extinction and backscattering coefficients) is related to the volume size distribution $\boldsymbol{v}$ as:

$$\mathbf{K}\boldsymbol{v} = \boldsymbol{g} \tag{2}$$

where $\mathbf{K}$ is the matrix containing discretized measurement kernels as columns.

Any particle bulk property $\boldsymbol{p}$ (for example, volume, surface, number density) can be estimated as:

$$\boldsymbol{p} = \mathbf{P}\boldsymbol{v} = \mathbf{P}\mathbf{K}^T\left(\mathbf{K}\mathbf{K}^T\right)^{-1}\boldsymbol{g}. \tag{3}$$

Here $\mathbf{P}$ is a matrix containing the weight coefficients for different integral properties as rows. For example for volume ($i = 1$) $P_{1k} = 1$, for surface ($i = 2$) $P_{2k} = \frac{3}{r_k}$ and for number density ($i = 3$) $P_{3k} = \frac{3}{4\pi r_k^3}$. It should be mentioned that when retrieving $\boldsymbol{p}$, we consider only projections of the characteristics of $\boldsymbol{p}$ on the measured set $\boldsymbol{g}$ and ignore the residual $\boldsymbol{p}_\perp$ that can not be measured directly with the available set of observations $\boldsymbol{g}$ (the so called null-space). Our previous results demonstrate that the existence of a null-space does not present a serious limitation to the LE technique for typical atmospheric aerosols (Veselovskii et al., 2012).

AMTD
6, 3059–3088, 2013

The inverse problem in our formulation is under-determined: the set of lidar measurements within a single atmospheric layer is limited – typically only 5 observations. This number of measurements is not sufficient to uniquely describe the properties of the aerosol, therefore, we use an intermediate approach. We perform inversions using a reasonable set of constraints and generate a family of solutions. Specifically, we consider a set of inversion windows $[r_{\min}, r_{\max}]$ and complex refractive indices $m = m_{\mathrm{R}} - i m_{\mathrm{I}}$ from the corresponding intervals. The limitations on the range of parameters variation can be considered as a priori constraints. Although those constraints do not provide a unique solution, they help to significantly reduce the number of solution family members.

Whatever approach we use for inversion (regularization or linear estimation) the key point is identifying a group of solutions which, after averaging, can provide a realistic estimation of particle parameters. Such identification can be done by considering the discrepancy ρ defined as the difference between input optical data $\boldsymbol{g}$ and optical data calculated from the solution obtained. In the linear estimation technique, we choose one optical datum g_p and estimate it from the rest of $N-1$ data using Eq. (3), as suggested in Graaf et al. (2010). By doing so for each optical data, we get N estimates of $\tilde{g}_p(m)$ that we compare with the observations g_p. And the discrepancy ρ is then calculated as:

$$\rho = \sqrt{\frac{\sum_p^N \left(g_p - \tilde{g}_p(m)\right)^2}{N}}. \tag{4}$$

Thus, the discrepancy quantifies inconsistency in input optical data. High discrepancy means that no appropriate particle parameters were found to generate optical data close to the observations $\boldsymbol{g}$. Normally a high discrepancy points to problems in the measurements, thus the discrepancy introduced here is a useful tool for the quality control of the input optical data.

As was pointed in our previous publication (Veselovskii et al., 2012), the high sensitivity of $\boldsymbol{g}$ to m allows the estimation of particle refractive index by calculating

AMTD
6, 3059–3088, 2013

$\Delta g_p = \tilde{g}_p - g_p$ for different assumed values of m and by searching for the minimum of the discrepancy. The estimation of the real part of the refractive index from the minimization of ρ in Eq. (4) is illustrated by Fig. 1 where the discrepancy ρ and the errors of volume estimation ε_V are given for different assumptions of m_R. Synthetic input data were generated assuming a log-normal distribution of particle number density $\frac{\mathrm{d}n(r)}{\mathrm{d}\ln r}$ with modal radius $r_0 = 0.15\,\mu\mathrm{m}$ and variance 0.4; the model refractive index is $m = 1.45 - i0.005$. As already mentioned, in the approach presented here the limitation of the range of parameters considered works as a constraint, thus there is dependence of $\rho(m_\mathrm{R})$ on the range of the values considered for the imaginary part $[0, m_{\mathrm{I,max}}]$. The computations in Fig. 1 were performed for values $m_{\mathrm{I,max}} = 0.01$, 0.02, 0.05. For an accurate estimation of m_R a strong dependence of $\rho(m_\mathrm{R})$ on this range of input values with a global minimum near the model value m_R is needed. Figure 1a demonstrates that for $m_{\mathrm{I,max}} = 0.01$ $m_\mathrm{R}(\rho)$ has minimum at the model value $m_\mathrm{R} = 1.45$ and the discrepancy rises for m_R above and below 1.45. However for larger $m_{\mathrm{I,max}}$ the minimum becomes wider, meaning that the accuracy of the estimation of m_R decreases and for $m_{\mathrm{I,max}} = 0.05$ it is practically flat from 1.45 to 1.65, so estimates of m_R in this range will have considerable uncertainty. Figure 1b shows the corresponding errors of volume estimation ε_V. It is interesting that, even though for the high values of $m_{\mathrm{I,max}}$, m_R cannot be determined with accuracy, the uncertainty of the volume estimation ε_V made using incorrect values of m_R does not increase significantly. From Fig. 1b we can conclude that $\varepsilon_V \approx 20\,\%$ when we choose $m_\mathrm{R} = 1.65$ instead of 1.45. The same is true for the rest of the parameters such as number, surface density and effective radius. So finally, the increase of the range of the values of m_I considered degrades the accuracy of the estimation of m_R, even though the rest of bulk properties can still be retrieved. Similar plots of $m_\mathrm{I}(\rho)$ can be provided to illustrate the estimation of the imaginary part of the refractive index. The corresponding simulation leads to the same conclusion: a reasonable estimation of m_I can only be made if preliminary information about the range of m_I variation is available.

AMTD
6, 3059–3088, 2013

The results presented in Fig. 1 were obtained assuming that the measurements contain no uncertainties. The introduction of uncertainty in the input data will modify $m_R(\rho)$ thus degrading the accuracy of the estimation of m_R. To analyze this effect, uncertainties were introduced in the synthetic input data in a random way in the range of 0–10 %. Figure 2 shows $m_R(\rho)$ plots for ten realizations following such a procedure assuming $m_{I,max} = 0.01$. $m_R(\rho)$ varies from realization to realization, still the uncertainty of the estimation of m_R is below ±0.05. The corresponding uncertainty of the volume density estimation does not exceed 20 %. These plots illustrate the possibility of estimating the real part of the refractive index from the measurements if we reasonably limit the range of values of m_I considered.

3 Results of the measurements

The multi-wavelength Mie–Raman lidar at NASA/GSFC is based on a Continuum 9050 laser with a 50 Hz repetition rate. The output powers at $\lambda = 355$, 532 and 1064 nm are 17.5, 7.5 and 14 W, respectively. The backscattered light is collected by a 40 cm aperture Schmidt–Cassegrain telescope operated vertically at 0.5 mrad field-of-view. The system is capable of detecting three backscattered signals at the laser wavelength and two nitrogen Raman signals at $\lambda_R = 387$ and 607 nm. The outputs of the detectors are recorded at 7.5 m range resolution using Licel transient recorders that incorporate both analog and photon-counting electronics. The full geometrical overlap of the laser beam and the telescope FOV is achieved at ∼ 1000 m, which determines the lower limit of the full set of our $3\beta + 2\alpha$ measurements due to the difficulty of calculating aerosol extinction in the overlap region.

For each profile, 6000 laser pulses were accumulated so the temporal resolution of the measurements was 2 min. The measurements were performed both in day and night time, but the full set of the measurements containing both backscattered and Raman signals could be acquired only in the nighttime. So in this paper only the results of the night time measurements are presented. The vertical profiles of the temperature,

AMTD
6, 3059–3088, 2013

and relative humidity were available from radiosondes launched at the Howard University research campus in Beltsville, MD, approximately 5 km away from GSFC.

One of the advantages of the LE approach is the possibility of reducing the number of input optical data and still performing reasonable retrievals of aerosol microphysical properties. Thus, instead of $3\beta+2\alpha$ measurements the reduced set of $3\beta+1\alpha$, where extinction at 532 nm is excluded, can be used (Veselovskii et al., 2012). Such data reduction does not lead to a significant degradation of retrieval accuracy at least when the fine mode dominates in the PSD and this situation is typical for the summer season in Maryland (Dubovik et al., 2002). This data reduction significantly simplifies data processing, because α_{532} determined from Raman nitrogen scattering with 2 min temporal resolution is characterized by significant uncertainty. But even for calculations of particle extinction at 355 nm from the Raman nitrogen signal, the height resolution is degraded to improve the signal to noise. In our calculations, the height resolution varied with height from 75 m (at 1000 m) up to 200 m (at 5000 m). All retrievals presented in this section were obtained from $3\beta+1\alpha$ measurements using the kernel functions for spherical particles.

To illustrate the application of the linear estimation technique for retrieval of time series of particle parameters, we have chosen measurements performed during the nights of 20–21 and 21–22 July 2011. For these nights, five-day backward-trajectories of the air-masses affecting the study area were calculated by the HYSPLIT-4 model. On 20–21 July night, at 500 and 1500 m the air-masses had their origins over the mid-West of the United States and followed a path through the areas of the Great Lakes inducing polluted aerosol loading mainly composed of sulphate particles. On the night of 21–22 July, the origin of the air-masses shifted to the southern US and the air-masses also followed a path over polluted areas near the Great Lakes.

3.1 21 July measurements

The structure of the PBL during the night of 20–21 July is illustrated by Fig. 3. The particle extinction at 355 nm is calculated by the Klett method (Klett, 1985) with 7.5 m

AMTD
6, 3059–3088, 2013

height resolution assuming the lidar ratio to be 70 sr, which was the average value of the lidar ratio derived from the Raman measurements. The Klett method was used to reveal finer variation in the structure of the PBL than would be retrievable using the Raman technique which requires more spatial and temporal averaging of the data. The top of the PBL is below 3500 m, though weak aerosol layers are observed up to approximately 4000 m. However, the optical density of these layers is too low for reliable computation of particle extinction and backscattering by the Raman method, so we limit the height range where the optical data are inverted to particle properties to altitudes less than 3200 m.

The spatio-temporal distribution of particle extinction at 355 nm calculated from the nitrogen Raman signal is shown in Fig. 4a. In the period from 00:40 UTC to 03:00 UTC a region of high aerosol loading, with extinction coefficient up to 0.4 km^{-1}, extended up to ~ 1400 m. Above that height α_{355} dropped to ~ 0.15 km^{-1}. After 03:00 UTC a second layer appeared at 2000 m and aerosols became distributed more uniformly through the PBL. The retrieved spatio-temporal distributions of the particle bulk parameters, such as volume density, effective radius and the real part of the refractive index are shown in Fig. 4b–d. The particle volume follows the extinction coefficient, meaning that the effective radius and the refractive index did not vary significantly. The retrieved effective radius (Fig. 4c) is about 0.25 µm at all heights. The real part of the refractive index is quite oscillatory in the region characterized by lower particle extinction (above 2000 m during 00:40–03:00 UTC) but after 03:00 UTC when aerosols are distributed more uniformly through the PBL, m_R becomes more stable and drops to approximately 1.4.

To quantify variations of the retrieved parameters, Fig. 5 shows the time-series of the volume, number density, effective radius and the real part of the refractive index in two layers of 200 m thickness centered at 1100 m and 2500 m where, inside of these layers, the parameters are averaged. The volume density at 1100 m drops from approximately 50 µm^3 cm^{-3} at 00:40 UTC to ~ 30 µm^3 cm^{-3} at 04:00 UTC, while V at 2500 m rises and after 04:00 UTC the volume densities in both layers have similar values. The number

AMTD
6, 3059–3088, 2013

densities behave in a like manner. Effective radii for both layers are also similar and slightly rise with time from 0.23 µm to 0.25 µm. The real part of complex refractive index (CRI) at 2500 m is larger than that in the 1100 m layer at 01:00 UTC, but by 05:00 UTC m_R in both layers is approximately 1.4. The absolute uncertainty of the effective radius and the real part of CRI retrieval we estimate to be 25 % and ±0.05, respectively, however the uncertainty of the relative change in the parameters should be lower, so we believe that the tendencies observed in the time-series in Fig. 5 are real. The imaginary part of the refractive index is about 0.006 and does not show significant variations during the night. It should be noted, however, that the uncertainty in the retrieval of m_I is high (about 50 % for $m_I > 0.005$) so any changes in m_I due to the uptake of water by the particles are beyond the sensitivity of the method.

3.2 22 July measurements

In contrast to 21 July the aerosol extinction on 22 July is characterized by significant variations. As we can conclude from Fig. 6, which shows particle extinction at 355 nm calculated by the Klett method using a lidar ratio of 70 sr, the top of the boundary layer drifts downward during the night from an elevation of 2.2 to 1.7 km. Between 03:30 UTC and 05:00 UTC a strong increase in extinction occurs, which is likely due to an intrusion of an external atmospheric layer. Figure 7 shows the spatio-temporal distribution of aerosol extinction at 355 nm calculated from the Raman nitrogen signal, and the retrieved volume density, effective radius, and real part of the refractive index. On the maps for r_{eff} and m_R the region with low particle extinction is removed (this region is marked in Fig. 7a with a solid line), because no reliable retrieval could be performed there. Again, as on 21 July, the variations of the volume density follow the particle extinction, while the effective radius is quite stable around a mean value of $r_{eff} \approx 0.25$ µm. Note that the enhancement of the particle extinction after 03:30 UTC does not have a significant effect on the effective radius values. The value of m_R inside the region with enhanced extinction (after 03:30) is lower, about 1.41, while outside that region m_R is about 1.43. To illustrate the variation of the particle parameters, Fig. 8 shows the time

AMTD
6, 3059–3088, 2013

series of volume, number density, effective radius and m_R for two height layers centered at 1200 and 1600 m. The thickness of the layers is 200 m. The particle volume density rises with time in both layers reaching a maximum value between 03:30 and 05:00 UTC. This enhancement correlates with the rise of the particle number density. At the same time, the effective radius is nearly constant at a value of approximately 0.26 µm. The real part of the refractive index in both layers slightly decreases after 03:00 UTC from 1.43 to 1.41. The vertical profiles of the particle backscattering coefficient at 355 nm and the effective radius retrieved are shown in Fig. 9 at 03:00 and 04:00 UTC, each profile is the result of 20 min of averaging. Both backscattering profiles show some variations, but the effective radius is quite stable.

4 Comparison with AERONET retrievals

To validate the retrievals made here by use of the linear estimation technique, we compared the lidar-derived effective radius and complex refractive index with the results provided by AERONET (Dubovik and King, 2000). The lidar profiles are available only above 1000 m and AERONET retrievals are column averages thus the two instruments are not measuring the same quantities. However the backscattering profiles did not show significant variations below 1000 m and above 1000 m the retrievals also do not show large variations. Therefore, we believe that such validation is reasonable in this case. In our sessions, the first lidar sounding started approximately 1.5 h after the last AERONET measurement so, given the generally stable conditions, we take the time gap to not be very significant.

Figure 10 shows the variations of effective radius and the real part of the refractive index provided by AERONET for 20–23 July period together with the results of lidar measurements. Effective radius did not change much during the day, and was about 0.25 µm for both 20 and 21 July, thus we can expect that this value of r_{eff} is preserved at the beginning of the lidar measurements also. The effective radius derived from the lidar measurements at 01:00 UTC on 20 and 21 July was about 0.24 ± 0.06 µm and

AMTD
6, 3059–3088, 2013

Retrieval of height-temporal distributions of particle parameters

I. Veselovskii et al.

0.26 ± 0.065 µm correspondingly, which is close to the AERONET values. The real part of the refractive index on 20 July provided by AERONET does not present significant spectral dependence and at 674 nm it varies between 1.39 and 1.46 during the day. The corresponding values obtained from lidar measurements at 01:00 UTC are in the range of 1.39–1.44 for different heights, as shown in Fig. 5. On 21 July the AERONET value of m_R is between 1.39 and 1.48, while lidar gives $m_R = 1.43 \pm 0.05$ at 01:00 UTC, as it is shown in Fig. 8. Thus both effective radius and the real part of CRI provided by the lidar and AERONET are in agreement.

One of the main AERONET products is the column-integrated particle volume. To get this same quantity from lidar measurements the volume density profile was extrapolated down to the ground, assuming that below a height of 1 km the volume density is constant. Figure 11 shows the time-series of the particle column volume obtained from lidar measurements on 21 July. The same figure shows the volume provided by AERONET at 23:00 for the total PSD and for the fine mode only. We present these two quantities as the lidar retrievals are known to be less sensitive to the coarse mode of the PSD. The particle column volume during the night varied from 0.075 µm^3 µm^{-2} to 0.1 µm^3 µm^{-2}, which is below the AERONET value 0.109 µm^3 µm^{-2} for the total PSD, but higher than the volume obtained for the fine mode only. Extrapolation of the lidar measurements to the ground can be a source of error, but still the agreement between lidar and AERONET derived values seems reasonable.

5 Conclusion

We have presented the results of application of the linear estimation technique to lidar measurements performed on summer 2011 at NASA GSFC. The intention of this research was to show that multiwavelength lidars are able not only to provide vertical profiles of particle properties but also to reveal the spatio-temporal evolution of aerosol features. The results obtained confirm that the LE algorithm operates stably and that time series of particle parameters measured with 2 min resolution provide useful results

AMTD
6, 3059–3088, 2013

without significant oscillations. We estimate the absolute accuracy of effective radius and the volume density retrieval as 25 % whereas we estimate the absolute accuracy for the retrieval of the real part of CRI to be ±0.05. Estimation of the imaginary part of CRI is possible only if we have some initial idea of the range of m_I variation. Long-term AERONET measurements demonstrate that aerosols over GSFC are generally low-absorbing and that m_I does not exceed 0.01 so this value can be used as a constraint under most conditions in the Greenbelt, MD area. For this situation m_I is estimated with an accuracy of 50 % in the range of 0.005–0.01.

An important part of the validation of the LE approach is the comparison with AERONET, which today is considered as one of the most reliable sources of column particle parameters. The comparison performed shows good agreement between the results obtained from the two instruments. The linear estimation approach proved to be also quite fast: the inversion of the whole night of measurements takes approximately 10 min using a standard PC. Thus, the LE technique used with multiwavelength HSRL or Raman systems has significant potential for air- and space-borne particle observations where data volumes can become quite large. Still more research are necessary to further validate the LE technique. Comparison of lidar measurements with AERONET and airborne in situ measurements should be performed at sites characterized by different types of particles and their mixtures and incorporation of spheroidal model is necessary to treat particles of irregular shape. Additional numerical simulations are also needed to estimate the retrieval uncertainties when contributions of the fine and the coarse mode are comparable. These considerations lead also to the question about input data reduction. Our results demonstrate that it is possible to exclude extinction at 532 nm from the input data while still providing a large amount of useful information about particle properties Still, additional studies are needed to verify that such data reduction can generally be done under a wide range of conditions. All these studies are areas for future research.

Acknowledgements. We would like to acknowledge the AERONET team at NASA/Goddard Space Flight Center in Greenbelt, MD for providing high-quality data and regular discussions of results.

References

Ansmann, A. and Müller, D.: Lidar and atmospheric aerosol particles, in: Lidar, Range-Resolved Optical Remote Sensing of the Atmosphere, edited by: Weitkamp, C., Springer, New York, 105–141, 2005.

Ansmann, A., Riebesell, M., Wandinger, U., Weitkamp, C., Voss, E., Lahmann, W., and Michaelis, W.: Combined Raman elastic-backscatter lidar for vertical profiling of moisture, aerosols extinction, backscatter, and lidar ratio, Appl. Phys. B, 55, 18–28, 1992.

Böckmann, C., Miranova, I., Müller, D., Scheidenbach, L., and Nessler, R.: Microphysical aerosol parameters from multiwavelength lidar, J. Opt. Soc. Am. A, 22, 518–528, 2005.

Burton, S. P., Ferrare, R. A., Hostetler, C. A., Hair, J. W., Rogers, R. R., Obland, M. D., Butler, C. F., Cook, A. L., Harper, D. B., and Froyd, K. D.: Aerosol classification using airborne High Spectral Resolution Lidar measurements – methodology and examples, Atmos. Meas. Tech., 5, 73–98, doi:10.5194/amt-5-73-2012, 2012.

De Graaf, M., Donovan, D., and Apituley, A.: Aerosol microphysical properties from inversion of tropospheric optical Raman lidar data, in: Proceedings of ISTP 8, 19–23 October 2009, Delft, the Netherlands, S06-O08, 2009.

De Graaf, M., Donovan, D., and Apituley, A.: Saharan desert dust microphysical properties from principal component analysis inversion of Raman lidar data over Western Europe, in: Proceedings of 25th International Laser Radar Conference, 5–9 July 2010, St. Petersburg, 671–674, 2010.

Donovan, D. and Carswell, A.: Principal component analysis applied to multiwavelength lidar aerosol backscatter and extinction measurements, Appl. Optics, 36, 9406–9424, 1997.

Draxler, R. R. and Rolph, G. D.: HYSPLIT (HYbrid Single-Particle Lagrangian Integrated Trajectory) Model access via NOAA ARL READY website http://ready.arl.noaa.gov/HYSPLIT.php, NOAA Air Resources Laboratory, Silver Spring, MD.

AMTD

6, 3059–3088, 2013

Dubovik, O. and King, M. D.: A flexible inversion algorithm for retrieval of aerosol optical properties from Sun and sky radiance measurements, J. Geophys. Res., 105, 20673–20696, 2000.

Dubovik, O., Holben, B. N., Eck, T. F., Smirnov, A., Kaufman, Y. J., King, M. D., Tanré, D., and Slutsker, I.: Variability of absorption and optical properties of key aerosol types observed in worldwide locations, J. Atmos. Sci., 59, 590–608, 2002.

Dubovik, O., Sinyuk, A., Lapyonok, T., Holben, B. N., Mishenko, M., Yang, P., Eck, T. F., Volten, H., Munoz, O., Veihelmann, B., van der Zande, W. J., Leon, J.-F., Sorokin, M., and Slutsker, I.: Application of spheroid models to account for aerosol particle nonsphericity in remote sensing of desert dust, J. Geophys. Res., 111, D11208, doi:10.1029/2005JD006619, 2006.

Ganguly, D., Ginoux, P., Ramaswamy, V., Dubovik, O., Welton, J., Reid, E. A., and Holben, B. N.: Inferring the composition and concentration of aerosols by combining AERONET and MPLNET data: comparison with other measurements and utilization to evaluate GCM output, J. Geophys. Res., 114, D16203, doi:10.1029/2009JD011895, 2009.

Hair, J. W., Hostetler, C. A., Cook, A. L., Harper, D. B., Ferrare, R. A., Mack, T. L., Welch, W., Izquierdo, L. R., and Hovis, F. E.: Airborne high spectral resolution lidar for profiling aerosol optical properties, Appl. Optics, 47, 6734–6752, 2008.

Holben, B. N., Eck, T. F., Slutsker, I., Tanre, D., Buis, J. P., Setzer, A., Vermote, E., Reagan, J. A., Kaufman, Y., Nakajima, T., Lavenu, F., Jankowiak, I., and Smirnov, A.: AERONET – a federated instrument network and data archive for aerosol characterization, Remote Sens. Environ., 66, 1–16, 1998.

Klett, J. D.: Lidar inversion with variable backscatter/extinction ratios, Appl. Optics, 24, 1638–1643, 1985.

Miller, D. J., Sun, K., Zondlo, M. A., Kanter, D., Dubovik, O., Welton, E. J., Winker, D. M., and Ginoux, P.: Assessing boreal forest fire smoke aerosol impacts on US air quality: a case study using multiple datasets, J. Geophys. Res., 116, D22209, doi:10.1029/2011JD016170, 2011.

Müller, D., Wandinger, U., and Ansmann, A.: Microphysical particle parameters from extinction and backscatter lidar data by inversion with regularization: theory, Appl. Optics, 38, 2346–2357, 1999.

AMTD
6, 3059–3088, 2013

Retrieval of height-temporal distributions of particle parameters

I. Veselovskii et al.

Müller, D., Kolgotin, A., Mattis, I., Petzold, A., and Stohl, A.: Vertical profiles of microphysical particle properties derived from inversion with two-dimensional regularization of multiwavelength Raman lidar data: experiment, Appl. Optics, 50, 2069–2079, 2011.
Nishizawa, T., Sugimoto, N., Matsui, I., Shimizu, A., and Okamoto, H.: Algorithms to retrieve optical properties of three component aerosols from two-wavelength backscatter and one-wavelength polarization lidar measurements considering nonsphericity of dust, J. Quant. Spectrosc. Ra., 112, 254–267, 2011.
Noh, Y. M., Müller, D., Mattis, I., Lee, H., and Kim, Y. J.: Vertically resolved lightabsorption characteristics and the influence of relative humidity on particle properties: multiwavelength Raman lidar observations of East Asian aerosol types over Korea, J. Geophys. Res., 116, D06206, doi:10.1029/2010JD014873, 2011.
Omar, A., Winker, D. M., Kittaka, C., Vaughan, M. A., Liu, Z., Hu, Y., Trepte, C. R., Rogers, R. R., Ferrare, R. A., Lee, K., Kuehn, R. E., and Hostetler, C. A.: The CALIPSO automated aerosol classification and lidar ratio selection algorithm, J. Atmos. Ocean. Tech., 26, 1994–2014, 2009.
Tesche, M., Ansmann, A., Müller, D., Althausen, D., Engelmann, R., Freudenthaler, V., and Groß, S.: Vertically resolved separation of dust and smoke over Cape Verde by using multiwavelength Raman and polarization lidar during SAMUM 2008, J. Geophys. Res., 114, D13202, doi:10.1029/2009JD011862, 2009.
Thomason, L. W. and Osborn, M. T.: Lidar conservation parameters derived from SAGE II extinction measurements, Geophys. Res. Lett., 19, 1655–1658, 1992.
Twomey, S.: Introduction to the Mathematics of Inversion in Remote Sensing and Linear Measurements, Elsevier, New York, 1977.
Veselovskii, I., Kolgotin, A., Griaznov, V., Müller, D., Wandinger, U., and Whiteman, D.: Inversion with regularization for the retrieval of tropospheric aerosol parameters from multi-wavelength lidar sounding, Appl. Optics, 41, 3685–3699, 2002.
Veselovskii, I., Kolgotin, A., Griaznov, V., Müller, D., Franke, K., and Whiteman, D. N.: Inversion of multi-wavelength Raman lidar data for retrieval of bimodal aerosol size distribution, Appl. Optics, 43, 1180–1195, 2004.
Veselovskii, I., Whiteman, D. N., Kolgotin, A., Andrews, E., and Korenskii, M.: Demonstration of aerosol property profiling by multi-wavelength lidar under varying relative humidity conditions, J. Atmos. Ocean. Tech., 26, 1543–1557, 2009.

Veselovskii, I., Dubovik, O., Kolgotin, A., Lapyonok, T., Di Girolamo, P., Summa, D., Whiteman, D. N., Mishchenko, M., and Tanré, D.: Application of randomly oriented spheroids for retrieval of dust particle parameters from multiwavelength lidar measurements, J. Geophys. Res., 115, D21203, doi:10.1029/2010JD014139, 2010.
Veselovskii, I., Dubovik, O., Kolgotin, A., Korenskiy, M., Whiteman, D. N., Allakhverdiev, K., and Huseyinoglu, F.: Linear estimation of particle bulk parameters from multi-wavelength lidar measurements, Atmos. Meas. Tech., 5, 1135–1145, doi:10.5194/amt-5-1135-2012, 2012.
Winker, D. M., Vaughan, M. A., Omar, A. H., Hu, Y., Powell, K. A., Liu, Z., Hunt, W. H., and Young, S. A.: Overview of the CALIPSO mission and CALIOP data processing algorithms, J. Atmos. Ocean. Tech., 26, 2310–2323, 2009.

AMTD
6, 3059–3088, 2013

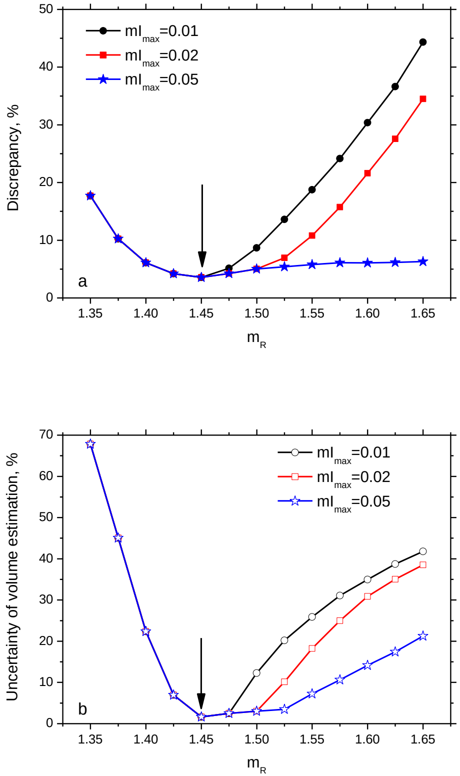

Fig. 1. (a) Discrepancy and **(b)** uncertainty of volume estimation as a function of assumed values of the real part of the refractive index for different ranges of considered values of the imaginary part with maximum values $m_I = 0.01, 0.02, 0.03$. The simulation was performed for a log-normal PSD with modal radius $r_0 = 0.15\,\mu m$ and dispersion $\ln\sigma = 0.4$. The arrow shows the real part of the refractive index $m_R = 1.45$ for the synthetic data.

AMTD
6, 3059–3088, 2013

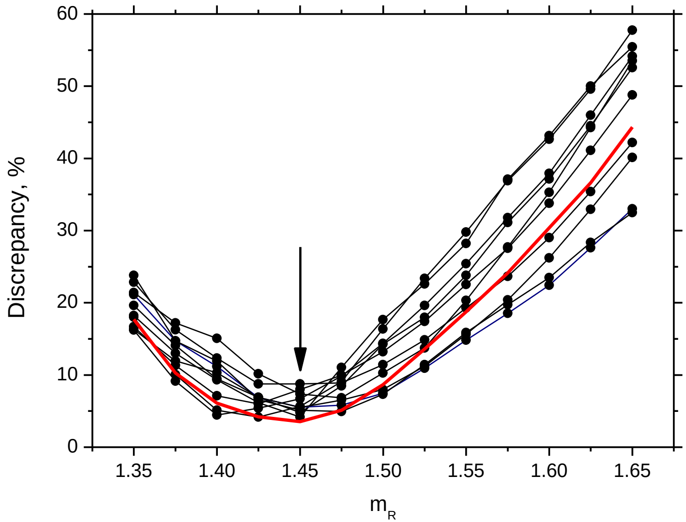

Fig. 2. Influence of random uncertainties in the input data on the discrepancy $\rho(m_R)$. The simulation was performed for the same parameters as in Fig. 1 and the maximum value of m_I was 0.01. The results are presented for ten realizations with random errors in the range of 0–10 %. The solid red line represents $\rho(m_R)$ in the absence of input errors; the arrow shows the model value of the real part of the refractive index $m_R = 1.45$.

AMTD
6, 3059–3088, 2013

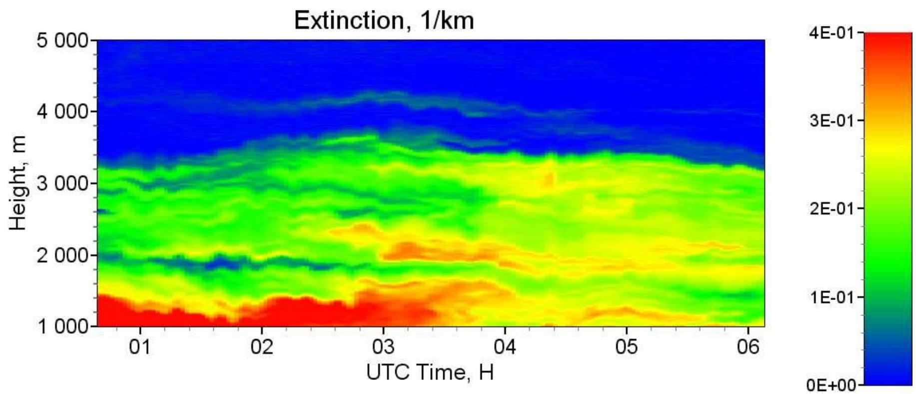

Fig. 3. Aerosol extinction at 355 nm on the night of 20–21 July calculated using the Klett method.

AMTD
6, 3059–3088, 2013

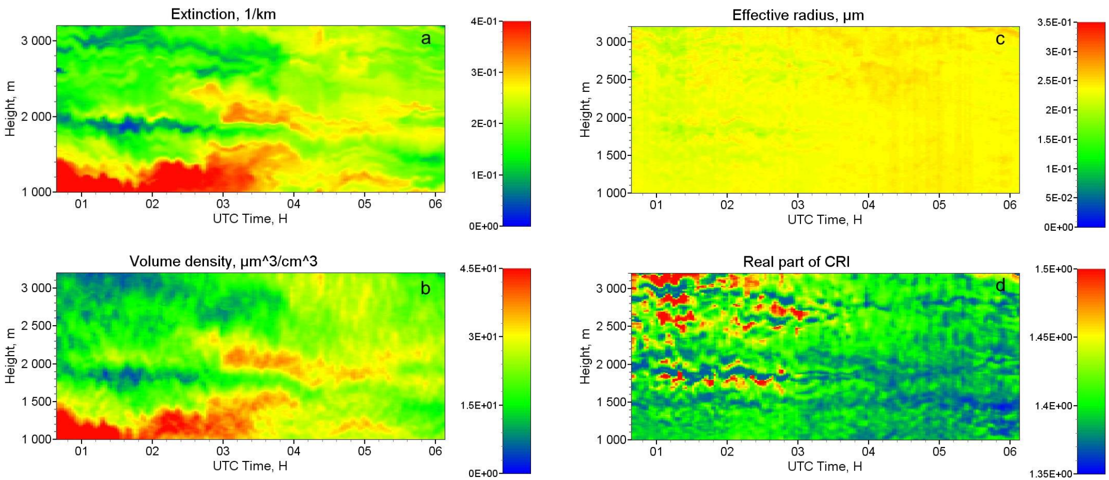

Fig. 4. Spatio-temporal distribution of **(a)** particle extinction at 355 nm calculated from the nitrogen Raman signal together with **(b)** particle volume, **(c)** effective radius and **(d)** the real part of the complex refractive index on 21 July 2011.

AMTD
6, 3059–3088, 2013

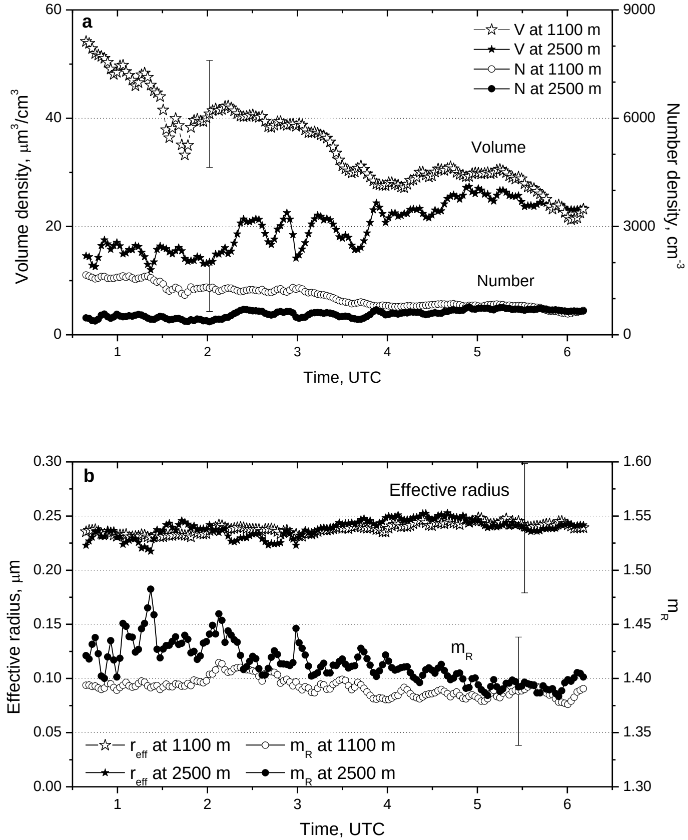

Fig. 5. Particle **(a)** volume, number density and **(b)** effective radius, real part of the refractive index obtained from lidar measurements on 21 July 2011. The lidar-derived parameters are averaged in layers of 200 m thickness and centered at 1100 m (open symbols) and 2500 m (solid symbols).

AMTD
6, 3059–3088, 2013

Retrieval of height-temporal distributions of particle parameters

I. Veselovskii et al.

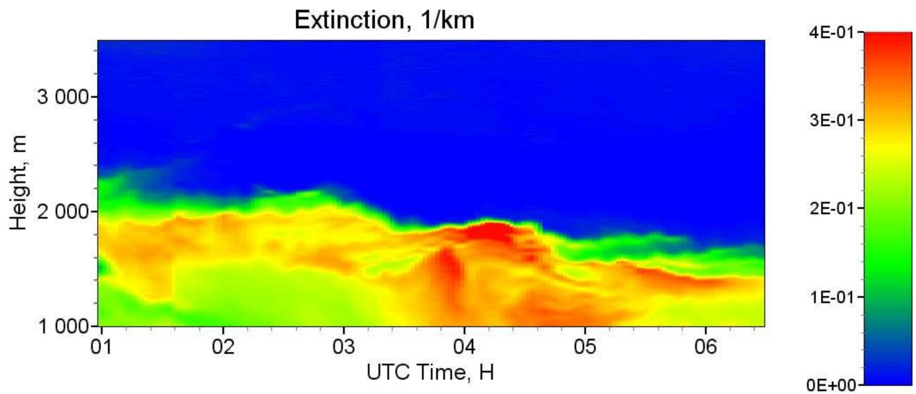

Fig. 6. Aerosol extinction at 355 nm on the night of 21–22 July calculated using the Klett method. The assumed lidar ratio is 70 sr.

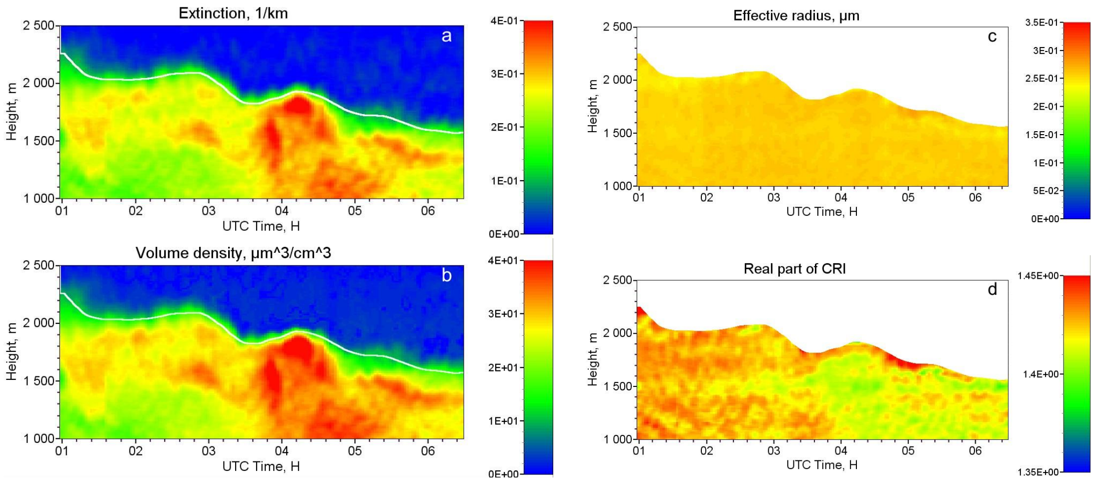

Fig. 7. Spatio-temporal distribution of **(a)** particle extinction at 355 nm calculated from the Raman nitrogen signal together with **(b)** particle volume, **(c)** effective radius and **(d)** the real part of the complex refractive index on 22 July 2011.

AMTD
6, 3059–3088, 2013

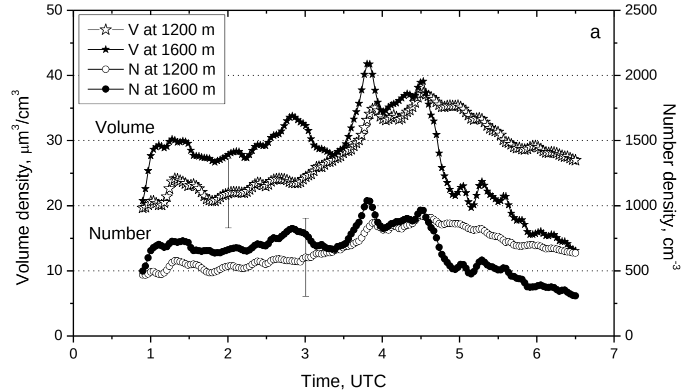

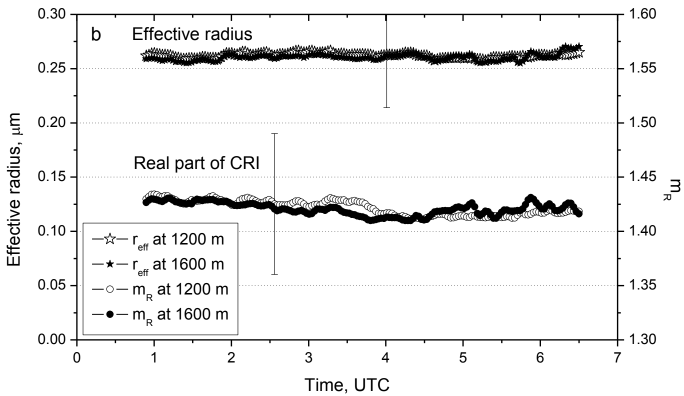

Fig. 8. Time series of **(a)** particle volume and number density together with **(b)** effective radius and the real part of the refractive index retrieved from the lidar measurements on 22 July 2011. The lidar-derived parameters are averaged in layers of 200 m thickness and centered at 1200 m (open symbols) and 1600 m (solid symbols) height.

AMTD
6, 3059–3088, 2013

Retrieval of height-temporal distributions of particle parameters

I. Veselovskii et al.

Title Page
Abstract Introduction
Conclusions References
Tables Figures
◀ ▶
Back Close
Full Screen / Esc
Printer-friendly Version
Interactive Discussion

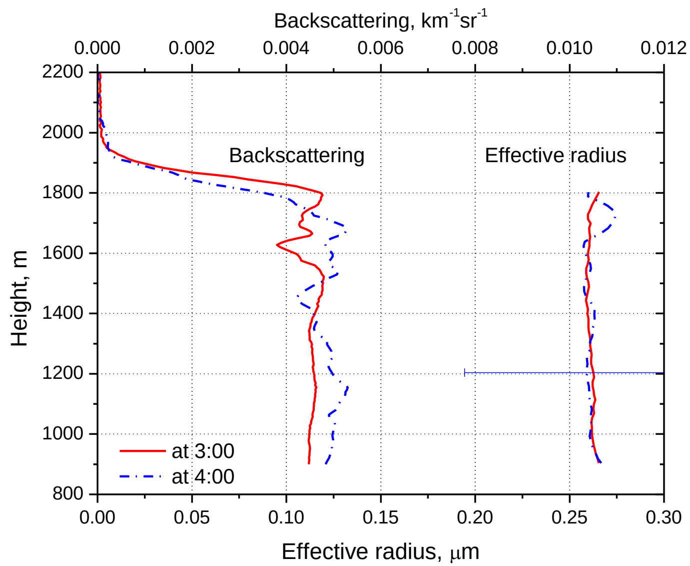

Fig. 9. Vertical profiles of particle backscattering at 355 nm measured at 03:00 UTC and 04:00 UTC together with retrieved profiles of effective radius.

AMTD
6, 3059–3088, 2013

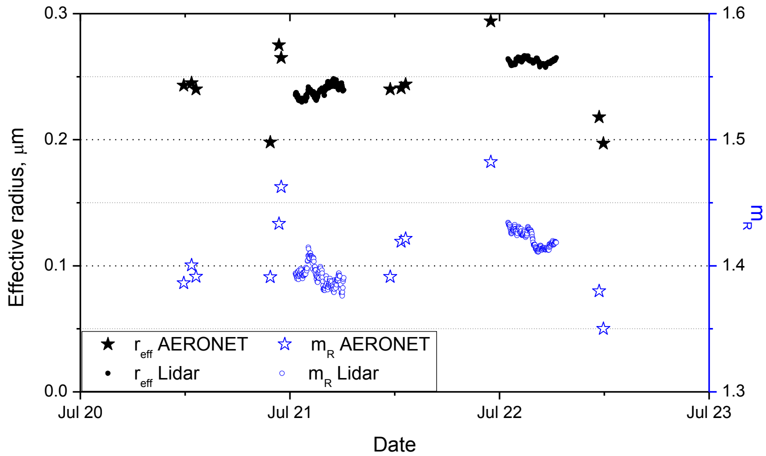

Fig. 10. Effective radius and the real part of the refractive index obtained from AERONET and lidar retrievals during the period of 20–23 July 2011. Lidar retrievals are shown for the height layers at 1100 m (21 July) and 1200 m (22 July).

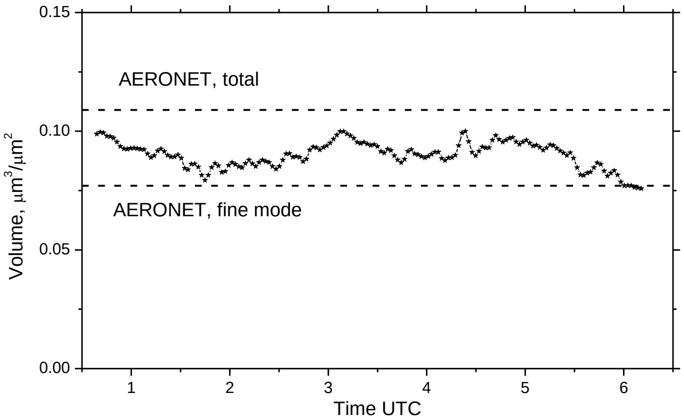

Fig. 11. Column-integrated particle volume retrieved from the lidar measurements on 21 July assuming a constant value of V below a height of 1 km. For comparison the column volume obtained from AERONET measurements at 23:00 UTC on 20 July for the total PSD and for the fine mode only are also given.